Experimental study of the heat transport processes in dusty plasma fluid

V. E. Fortov,[1] O. S. Vaulina,[1] O. F. Petrov,[1] M. N. Vasiliev,[2] A. V. Gavrikov,[1] I. A. Shakova,[1] N. A. Vorona,[1] Yu. V. Khrustalyov,[1] A. A. Manohin,[2] and A. V. Chernyshev[1]

[1]*Institute of High Energy Densities JIHT RAS, Moscow, 125412, Russia*

[2]*Moscow Institute of Physics and Technology, Moscow, Russia*

(Received 24 March 2006; revised manuscript received 29 September 2006; published 16 February 2007)

The results are given of an experimental investigation of heat transport processes in fluid dusty structures in rf-discharge plasmas under different conditions: for discharge in argon, and for discharge in air under an action of electron beam. The analysis of steady-state and unsteady-state heat transfer is used to obtain the coefficients of thermal conductivity and thermal diffusivity under the assumption that the observed heat transport is associated with a thermal conduction in the dusty component of plasmas. The temperature dependence of these coefficients is obtained, which agrees qualitatively with the results of numerical simulation for simple monatomic liquids.

DOI: 10.1103/PhysRevE.75.026403 PACS number(s): 52.27.Lw, 52.27.Gr

I. INTRODUCTION

The physical properties of nonideal dissipative systems are of significant interest in various fields of science (hydrodynamics, plasma physics, medicine, etc.) [1–5]. The major problem encountered in studying such systems is associated with the absence of an analytical theory of liquid that would be capable of explaining its thermodynamic properties, describing the heat and mass transfer, etc. Two basic approaches are employed in developing approximate models for liquids, the first one of which consists in numerical calculation of properties of a medium using model data on the particle interaction [6–15]; the second method is based on analogies between the crystalline and liquid states of matter [1–4]. The difficulty of checking the suggested models is that the spectrometric diagnostics of a liquid are often very inexact [2–4]. Unlike real liquids, laboratory dusty plasma is a good experimental model for studying the nonideal systems [16–18]. This plasma is a partly ionized gas with charged dust macroparticles ($\sim 1-10$ μm in size), which may be observed by a video camera; this enables one to investigate the processes of heat and mass transfer at the kinetic level.

The majority of numerous investigations of dusty plasma are based on the model of screened Coulomb potential $U=(eZ)^2\exp(-r/\lambda)/r$, where r is the interparticle spacing, λ is the screening length, and eZ is the charge. The screening intergrain interactions were observed experimentally for grains trapped in the electric field of capacity rf-discharge [19], in inductive rf-discharge [20], and in dc-glow discharge also [21]. It should be noted that this (Debye) model for intergrain interactions may be incorrect under conditions of a dense grain cloud and in the sheath region of laboratory gas discharges, as well as this model does not take into account the ionization/recombination processes, the collisions of plasma electrons and ions with neutrals, and many other factors [22].

Two dimensionless parameters responsible for the mass transfer in such systems were found in [10–12] for $\kappa=r_d/\lambda<6$, where $r_d=n_d^{-1/3}$ is the mean interparticle spacing, and n_d is the concentration. These are the effective coupling parameter $\Gamma^*=(Ze)^2/(Tr_d)\{(1+\kappa+\kappa^2/2)\exp(-\kappa)\}$ (which defines the form of the pair correlation function from $\Gamma^*\sim 1$ to the crystallization point $\Gamma^*=\Gamma^*_c\cong 102$) and the scaling parameter $\xi\equiv\nu_{fr}/\omega^*$, where $\omega^*=eZ\{(1+\kappa+\kappa^2/2)\exp(-\kappa)/(r_d^3\pi M)\}^{1/2}$ is the characteristic frequency ω^* of charged particles, ν_{fr} is the effective frequency of their collisions with neutrals of surrounding gas [23], and M and T denote the mass of a dust particle and kinetic temperature of a dusty component (in energy units).

In presented work the results of an experimental investigation of processes of heat transport are given for fluid dust structures in plasma of a capacitive radio-frequency (rf-) discharge under different conditions: for rf-discharge (in argon); and for RF-discharge (in air) under an action of electron beam. Experiments were performed for macroparticles with different sizes (~ 0.5 and 2 μm in radius), and material (Al_2O_3 and latex). The analysis of steady-state and unsteady-state heat transfer is used to obtain the coefficients of thermal conductivity and thermal diffusivity under the assumption that the observed heat transport is associated with a thermal conduction in the dusty component of plasmas. Possible mechanisms of heat transport in experiments presented are considered. Comparison of experimentally retrieved constants of heat transfer with numerical data for simple monatomic liquids is given.

II. RELATIONS BETWEEN TRANSPORT CONSTANTS FOR SIMPLE FLUIDS

The coefficients of diffusion D, thermal conductivity χ, and viscosity η reflect the thermodynamic state of a system. In the case of gases, the constants of diffusion, kinematical viscosity $\nu=\eta/\rho$, and thermal diffusivity $\theta=\chi/(\rho c_p)$ are close in value and may be written in the form of known analytical relations [23] (here, $\rho=M n_d$, and c_p is the specific heat capacity at constant pressure P). Such relations for the liquid state of matter enable one to employ known hydrodynamic models for analysis of the wave propagation, the formation of vortexes and various instabilities in highly nonideal media. The numerical simulation of transfer processes in simple monatomic liquids with a wide scope of interaction

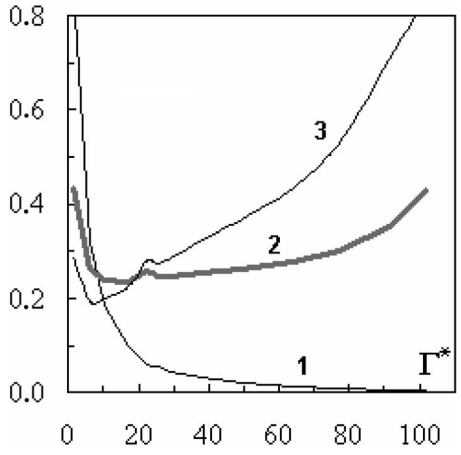

FIG. 1. Normalized transport constants D^* (**1**), ν^* (**2**), and θ^* (**3**) vs Γ^* for the systems with the screened Coulomb potential.

potentials reveals that the relations between the transport coefficients may be approximated as [4]

$$\eta \cong T/(8.1 r_d D), \tag{1}$$

$$\theta \cong \frac{0.75 k_B}{M c_p} r_d V_t \left(\frac{0.6 r_d V_t}{D}\right)^{5/8}, \tag{2}$$

where $c_p = 2.5 k_B/M$, and k_B is the Boltzmann constant. The main difference between the properties of simple liquids and plasma-dust systems is associated with the presence of dissipation of the energy of dust particles due to their collisions with neutral gas. In the case of weakly dissipative systems ($\nu_{fr} \ll \omega^*$, $\xi \to 0$), the results of simulation of the dynamics for macroparticles and simple liquids coincide. In order to include the dissipation, the coefficient of diffusion must be reduced by a factor of $(1+\xi)$, and the viscosity coefficient must be accordingly increased by $(1+\xi)$ [10,12]. No experimental or numerical data have been available heretofore on the effect of the friction forces on the heat transfer in nonideal systems. Nevertheless, if we rely on Eq. (2) and take into account the fact that $D \propto 1/(1+\xi)$, the values of heat transfer coefficients in dissipative systems must exceed their values for the dispersion case by a factor of $(1+\xi)^{5/8}$. The values of normalized transport constants, $D^*(\Gamma^*) = D(1+\xi)/(\omega^* r_d^2)$ and $\nu^*(\Gamma^*) = \nu/[(\omega^* r_d^2)(1+\xi)]$, for the systems with the screened Coulomb potential are shown in Fig. 1 (from numerical data of studies [9,10,12–15]). In this figure the normalized value of thermal diffusivity $\theta^* = \theta/[(\omega^* r_d^2)(1+\xi)^{5/8}]$ [retrieved from Eq. (2), and the diffusion simulations] is also shown. [Notice that in the case of weakly dissipative systems ($\xi \to 0$): $D^* \to D/(\omega^* r_d^2)$; $\nu^* \to \nu/(\omega^* r_d^2)$; $\theta^* \to \theta/(\omega^* r_d^2)$.] The presented curves illustrate the limits of the constant relation between the transport coefficients η and χ that is often used in analysis of properties of simple liquids: $\eta \approx c_p\ \chi = 2.5 k_B/M\chi$ ($\nu \approx \theta$) [4]. Taking into account that the errors under numerical simulations are some 20%, this relation is suitable for values of Γ^* from ~4 to ~40 (see Fig. 1).

III. HEAT TRANSFER EQUATIONS

In the case of heat transfer (no convection), the heat flux density $\boldsymbol{q}$ obeys the Fourier law [24]

$$\mathbf{q} = -\chi \nabla T/k_B, \tag{3}$$

where $\boldsymbol{q} = 0.5[\int \boldsymbol{V} M V^2 \mathrm{d}N]/S\delta x$ is the heat flux transferred by particles at velocity $\boldsymbol{V}$ through an area S of a layer of matter of thickness δx, and N is the number of particles. In the absence of vibrations and rotation of particles and assuming their energy to be uniformly distributed over the degrees of freedom, the density of heat flux propagating in the preferred direction $\mathbf{x}$ may be found as $q \approx 1.5\rho(\langle V_x^3\rangle_+ - \langle V_x^3\rangle_-)$, where $1.5\rho\langle V_x^3\rangle_{+(-)}$ is the amount of heat transferred in the direction of $(+)$ and counter to $(-)$ the flow. Then, one can write for the coefficient χ

$$\chi \approx 1.5 n_d \delta x k_B (\langle V_x^3\rangle_+ - \langle V_x^3\rangle_-)(\langle V_x^2\rangle_+ - \langle V_x^2\rangle_-)^{-1}. \tag{4}$$

[In this case the thermal diffusivity may be obtained as $\theta = \chi/(\rho c_p) \cong 2\chi/(5n\ k_B)$.]

The nonuniform distribution of the dust temperature in plasma (including a highly nonisotropic distribution) is observed quite frequently [25–27]. This phenomenon may be explained by spatial variation of dust charges, which provides for the formation of internal heat sources, Q_h, in a system. Because Eqs. (3)–(5) are valid for an inhomogeneous medium as well; a possibility exists of obtaining the temperature dependence of heat-transfer coefficients.

The heat transfer equation in a stationary medium (without convection, or another regular motion), where an energy transport is the result from the thermal conductivity only, may be written as [24]

$$\partial T/\partial t = \{\mathrm{div}\ \chi \nabla (T) + k_B Q\}/\{c_p \rho\}. \tag{5}$$

Here $Q = Q_h + Q_d$ is the source function which can be presented as a superposition of the internal natural heat sources, Q_h, and the internal sources of energy dissipation, Q_d (the heat discharge). Taking into account that the basic source of dissipation of the energy of dust particles in weakly ionized plasma is their collisions with neutral gas, we can assume (for the case of one-dimensional heat transfer) [17]

$$k_B Q_d/(c_p \rho) = 2\nu_{fr} T. \tag{6}$$

The steady-state distribution of temperature ($\partial T/\partial t = 0$) obeys the equation $\mathrm{div}\ \chi \nabla T = -Q$. In the case of uniform spatial distribution of T ($\nabla T = 0$), the value of $Q = 0$ and $Q_d = Q_h$. The mechanisms of a formation of heat sources, Q_h, for dust particles in plasma may be various, including the space-time fluctuations of the dusty plasma parameters [25–30] (e.g., the macroparticle charges) as well as development of various plasma-dust instabilities in the electric fields of the gas-discharge chambers [27,31,32]. In doing so, with the different mechanisms of dust heating, the stochastic thermal motions of dust particles may result from the small perturbations of systems (self-excited oscillations) or can appear with a growth of displacements of dust particles from its equilibrium positions above the some critical amplitude [26].

Notice that the time of the formation of different plasma-dust instabilities (leading to the dust heating) is usually close

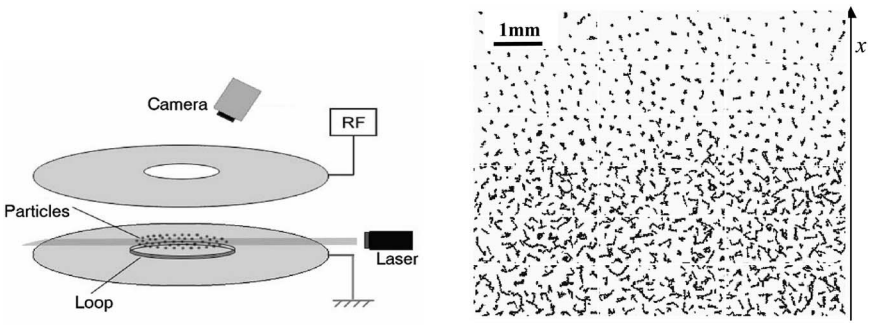

FIG. 2. The scheme of the experiment (a) and video image of stable two-phase dust structure (b) with the trajectories of separate particles for time $t=0.25$ s.

to the time of the dust charging ($\sim 10^{-4}-10^{-6}$ c). In this case the time of the dust heating, due to the formation of these instabilities, is determined by the time of the thermalization of the system (by the time for the establishment of Maxwell's distribution for dust velocities) [23,33]

$$\tau_{\mathrm{Max}w} \cong \nu_{\mathrm{fr}}/\omega_d^2, \tag{7}$$

where $\omega_{\mathrm{d}}^2=4\pi(eZ)^2 n_{\mathrm{d}}/M$. For this time the mechanisms (that produce the dust heat sources, Q_{h}) are balanced by the mechanisms of dissipation of dust energy in the systems. Thus, because in terms of macroscopic kinetics, Eq. (5) is valid only at a physically long time scale in the case of $\tau_{\mathrm{eq}} \gg \tau_{\mathrm{Max}w}$ (where τ_{eq} is the time of equalization of temperature in the analyzed system [23,33]), we may assume that in the presence of the above-mentioned mechanisms of dust heating, the dissipation sources, Q_{d}, must be balanced by heat sources, Q_{h} ($Q_{\mathrm{d}} \approx Q_{\mathrm{h}}$). Examination of this assumption is presented in Sec. III.

A set of problems for a theory of heat transfer are the tasks on determination of velocities of equalization of temperature for nonuniform heated finite media, the surface of which is under preassigned conditions. For these tasks a general solution of the heat equation is usually used in the form [24]

$$T(\boldsymbol{x},\mathrm{t}) = \sum c_{\mathrm{n}} T_{\mathrm{n}}(\boldsymbol{x}) \exp(-\lambda_{\mathrm{n}} t), \tag{8}$$

where c_{n} are some constants, T_{n} obey the equation

$$\theta \Delta T_{\mathrm{n}} = \lambda_{\mathrm{n}} T_{\mathrm{n}}, \tag{9}$$

and λ_{n} (with $n=1,2,3,\ldots$) are the set of the special values where Eq. (9) has a solution under preassigned boundary conditions. Notice that the velocity of equalization of temperature determines by minimal value of $\lambda_{\mathrm{n}}=\lambda_1$, and the time τ_{eq} for this temperature equalization can be presented as $\tau_{\mathrm{eq}}=1/\lambda_1$ [24].

Finally we note that in the case of dissipative dust structures (with $\xi \gg 1$) Eqs. (3)–(5) do not allow a determination of these coefficients (χ, θ) for a pure dust component; the influence of buffer gas (friction coefficient) must be taken into account as pointed out in the end of Sec. II, according to the existing models developed in the statistical theory of liquid [4].

IV. EXPERIMENTS IN rf-DISCHARGE

The experiments on a study of heat transfer were performed in plasma of a capacitive radio-frequency discharge in argon ($P \approx 20$ Pa) with Al_2O_3 particles 3–5 μm in diameter (average radius $a_{\mathrm{d}} \approx 2$ μm and density $\rho_{\mathrm{d}} \approx 2.4$ g cm^{-3}) that were trapped in a confined electric field of the gas discharge chamber. The scheme of experiment is given in Fig. 2(a). For diagnostic purposes, the particles of a dust cloud were illuminated by a plane beam of a He-Ne laser. The illumination was performed in two ways. In the first case we have used a nonfocused laser beam that allowed the determination of the total geometric size of the dust cloud. In the second case the diagnostics involved the illumination of the horizontal monolayer of the dust cloud by a laser sheet (thickness ~ 250 μm) for detailed study of dust structures and their dynamics. The analyzed monolayer was filmed using a charge coupled device camera (frame frequency, 50 s^{-1}). Analyses were performed for 5–7 horizontal dust layers placed close to the center of a dust cloud. Diagnostics of the vertical structure of a dust cloud involved the illumination of their vertical cross sections by the laser sheet. The video records were treated using special computer codes. The coordinates and trajectories of particles were obtained as a result of video records processing.

Under the experiments, the dust cloud was initially an equilibrium liquid structure consisting of $\sim 13-15$ dust layers ~ 3.5 cm in diameter. As a result of minor variation of the discharge parameters (increase in power or decrease in pressure), one of the cloud edges was heated rapidly. (This asymmetric perturbation is caused by the geometric nonuniformity of the trap.) The front of the propagation of thermal perturbation was flat; the perturbation propagated in the single (horizontal) direction **x** [see Fig. 2(b)]. We have not registered any temperature gradients in other directions. Here it should be noted that the technique of direct visualization of dust particles allows the registration of any changes in their translational degrees of freedom. We have also observed no dust drifts or convections in analyzed structures for stationary cases as well as for unsteady-state heat transport. (Distributions of dust velocities were close to Maxwell's functions.)

The thermal perturbation propagated through the dust structure in the horizontal direction during ~ 12 to 13 s. Then the dust system aroused a new equilibrium state with a clearly defined interface between the low-temperature and

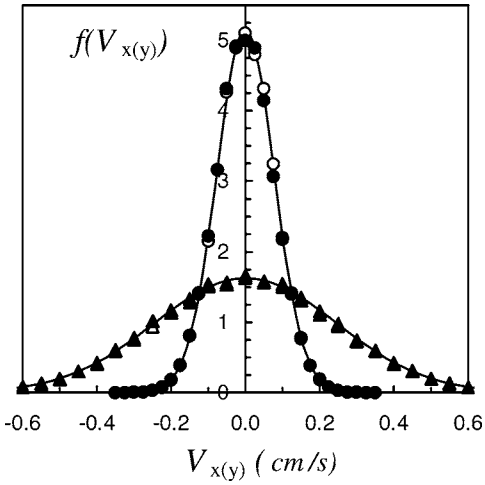

FIG. 3. Macroparticles' velocity distributions for the high-temperature (▲, △) and low-temperature (●, ○) regions: (▲, ●)–$f(V_x)$; (△, ○)–$f(V_y)$. Continuous lines are the Maxwell curves for measured temperatures of the dusty component. $T=3$ and 0.3 eV, accordingly.

high-temperature regions [see horizontal cross section of dust cloud in Fig. 2(b)] and during another ~300 s the characteristics of the observed dust structure were held practically constant. The parameters of the high-temperature region were as follows: $T\approx 3$ eV, $r_d\approx 400$ μm, $\Gamma^*\approx 6$, $\omega^*=(T\Gamma^*/(\pi M r_d^2)\}^{1/2}\approx 8.5$ s^{-1}. The low-temperature region exhibited characteristics close to the parameters of an unperturbed system: $T\approx 0.3$ eV, $r_d\approx 500$ μm, $\Gamma^*\approx 49$, $\omega^*\approx 6.8$ s^{-1}. In all cases the registered dust concentration was close to the constants ($r_d\approx 400$ μm) for the temperatures $T>0.7$ eV, with decreasing of T it was about halved. The temperature was analyzed using the measurements of the dust velocity distributions (see Fig. 3); the mean distance r_d and parameter Γ^* were determined from the experimental pair correlation function (see Fig. 4). The measured errors in temperatures and Γ^*, were about 10%, the errors in determination of r_d were less than 5%. The friction coefficient was

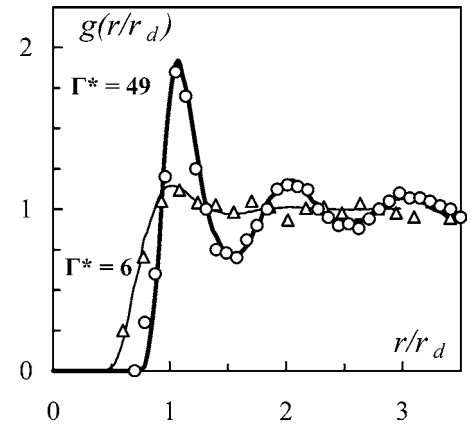

FIG. 4. Experimental pair correlation functions $g(r/r_d)$ for △–high-temperature, and ○–low-temperature regions. Continuous lines are the results of numerical simulations for the appropriate Γ^* parameters.

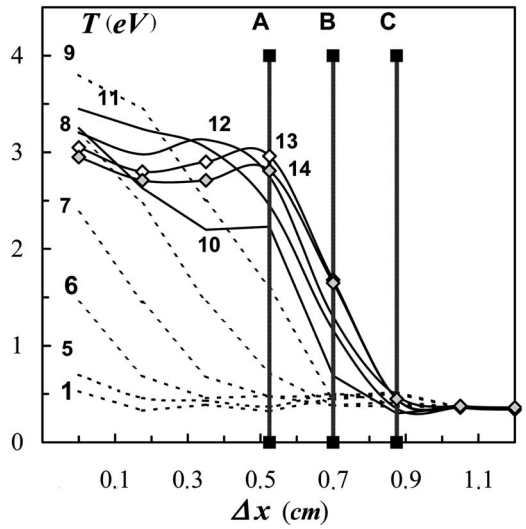

FIG. 5. Spatial distribution of thermal perturbation for different times of observation. The numerals indicate the time in seconds; $\Delta x=m\delta x$, where m is the number of analyzed regions of width δx. Vertical lines show the regions of measurement of χ in the steady state.

$\nu_{fr}\approx 35$ s^{-1} (in a free-molecular approach for $a_d\approx 2$ μm [23]).

As mentioned above the nonuniform distribution of the dust temperature (including highly nonisotropic distributions like those observed) is found quite frequently in a gas discharge plasma [25–27]. For most cases this phenomenon may be explained by spatial variation of dust charges, which provides for the formation of internal heat sources in a system. A formation of two-temperature dust structures from an initial homogeneous cloud with a variation of experimental conditions in our experiments can be explained by the mechanism proposed in [26] where the physics of the dust "heating" in the systems with small spatial variation of dust charge (due to the perturbations of these systems with an amplitude more than its critical value) was detailed. It should be noted that Eqs. (3)–(5) do not have restrictions on any mechanisms of heating or ways of formation of internal heat sources. A validity of these equations above all is determined by the fact that the observed heat transport must be induced by the temperature gradients via the heat conduction. Because the analysis of the measured dust velocity distribution has not revealed any convective (or another regular) motion in analyzed structures (see above), we can suppose that both convections and diffusions are lacking in our experiments, and that the observed heat transport is associated with a thermal conduction in the dusty component of plasmas.

The results of determining the conductivity χ using Eq. (4) for steady-state conditions ($t>13$ s) on the interface for the A-C region of width $\sim 2\delta x=0.35$ cm and, separately, for the A-B and B-C regions (see Fig. 5) are given in the Table I as functions of the average (for these regions) temperature. The errors in measured values of χ were about 10%. Also given in this table are the values of $\theta=2\chi/(5n_d k_B)$ and parameter Γ^* which was obtained by simple scaling of its value for the high-temperature region.

In order to analyze the dust medium during the motion of thermal perturbation, the video frame was divided into sev-

TABLE I. Coefficients θ and χ for steady state of a dust structure in rf-discharge.

T (eV)	Γ^*	$\chi 10^{14}$ (erg/(s cm K))	θ (cm^2/s)
2.7 [A;B][a]	6.7	2.39	0.011
1.68 [A;C]	10.7	2.16	0.010
1.3 [B;C]	13	1.93	0.0089

[a]The location of analyzed region of dust structure (see Fig. 4) is shown in brackets.

eral rectangular regions of width $\delta x \approx 0.175$ cm. The pattern of motion of the front of thermal perturbation, obtained by averaging the temperature of dusty particles in these regions, is given in Figs. 5 and 6. One can readily see that the boundaries of the heated region expand during ~8 s after thermal perturbation. Then, the velocity of motion of the front decreases abruptly, and the kinetic energy of particles experiences a new perturbation which is possibly caused by the "collision" of the thermal front with the region where a formation of the internal heat sources occurs. After another ~4 to 5 s, the dust system assumed a new equilibrium state and represented a liquid two-temperature medium with a clearly defined interface between the low-temperature and high-temperature regions at a distance of ~2–2.5 cm from the site of initiation of thermal perturbation [see Figs. 2(b) and 5 the regions with $\Delta x > 0.9$ cm, and with $\Delta x > 0.5$ cm, respectively, at the time ~13 to 14 s). All experimental values presented here are the result of averaging of data for four repeated experiments.

Let us consider a dynamics of observed propagation of thermal perturbation in our experiments. As mentioned above, the analysis of measured dust velocity distribution has not revealed any convective (or another regular) motion in analyzed unsteady-state heat transport, we can assume that the propagation of a temperature front observed in our experiments may be associated with a thermal conduction. For examination of this assumption we can estimate approximately the time of equalization of temperature τ_{eq} in our

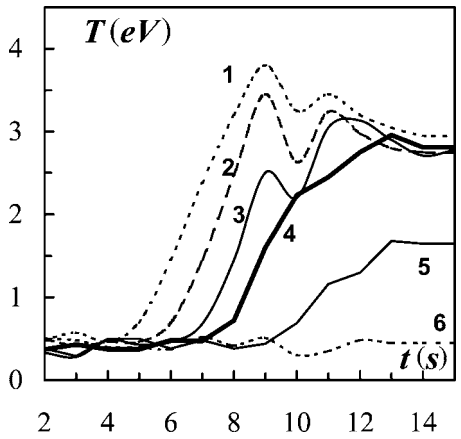

FIG. 6. The dust temperature T as a function of time t in different regions of a structure Δx: (**1**) 0, (**2**) 0.175 cm, (**3**) 0.35 cm, (**4**) 0.525 cm, (**5**) 0.7 cm, and (**6**) 0.875 cm.

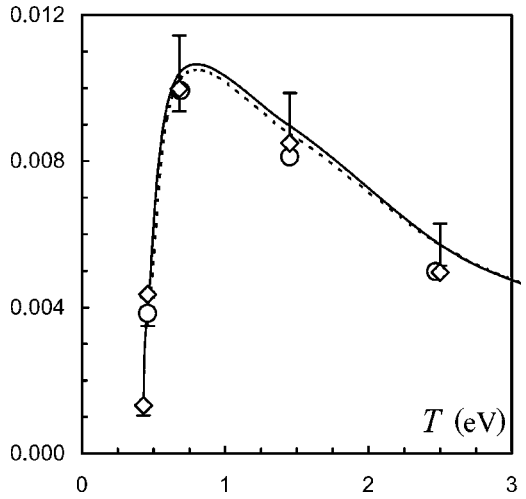

FIG. 7. Experimental values of $(\partial T/\partial t)/q_d$ (lines), and the results of the best fitting of $(\partial T/\partial t)/q_d$ by the functions $\propto A\Delta T/q_d$, where $A=0.014$ cm^2/s (symbols) vs T for different regions of dust structure Δx: (hard line; ◇) 0; (dashed line; ○) 0.35 cm.

experiments using the values of the thermal diffusivity θ coefficients obtained in steady-state conditions $\theta \approx 0.01$ cm^2/s (see Table I). The order of magnitude of τ_{eq} may be obtained from the solution of the problems (8) and (9) for a plane-parallel slab with thickness L: $\tau_{eq}=L^2/(\pi^2\theta)$ [20]. Then, for the characteristic length in the direction of heat propagation $L \approx 0.5$ cm we can derive $\tau_{eq} \approx 5$ c that is in agreement with the experimental observation (see Fig. 5). Additional estimation of the thermalization time gives $\tau_{Maxw} \cong \nu_{fr}/\omega_d^2 = \nu_{fr}/(2\pi\omega^*)^2 \sim 0.01$ c that is well above the time of equalization of temperature τ_{eq} in analyzed volume of dust cloud.

Thus we can use Eq. (5) for analysis of heat transport in our experiments in unsteady-state conditions by analyzing the motion of the wave front for $t \leqslant 8$ s and $\Delta x \leqslant 0.525$ cm. Experimental values of $\partial T/\partial t$ divided by $q_d=2\nu_{fr}T$ (where $\nu_{fr}=35$ s^{-1}) are presented in Fig. 7 versus T for different regions of dust structure. The results of the best fitting of $(\partial T/\partial t)/q_d$ functions by the functions $\propto A\Delta T/q_d$, with the constant $A=0.014$ cm^2/s, are also shown in Fig. 7. We can easily see that the difference between these functions is within 15%. Analysis of results of measurements show also that both the $\partial T/\partial t$ [that is the left part of Eq. (5)] and ΔT functions are practically independent on x within the analyzed part of the dust structure. The behavior of these functions is determined by the dust temperature, T. Taking into account the Q_d function, Eq. (6), we can assume that the heat sources, Q_h, are also the function of T, in doing so $Q_h \approx Q_d$ as $(\partial T/\partial t)/q_d \leqslant 1$. Recall also, that under initial state, $\nabla T=0$, as well as under final steady-state conditions ($\nabla T=0$, $T \approx \text{const}=3\pm0.15$ eV for $\Delta x \leqslant 0.525$ cm.) the $\partial T/\partial t$ value is equal to 0, and $Q_h=Q_d$. Then, assuming that the effect of sources function may be ignored ($Q_h=Q_d$), we can estimate the coefficient of thermal diffusivity, $\theta=\chi/(\rho c_p) \approx A=0.014$ cm^2/s. In this case the difference between the $\partial T/\partial t$ and $A\Delta T$ functions (~±15%) may be determined by the temperature dependence of $\theta=\theta(T)$. Nevertheless we cannot

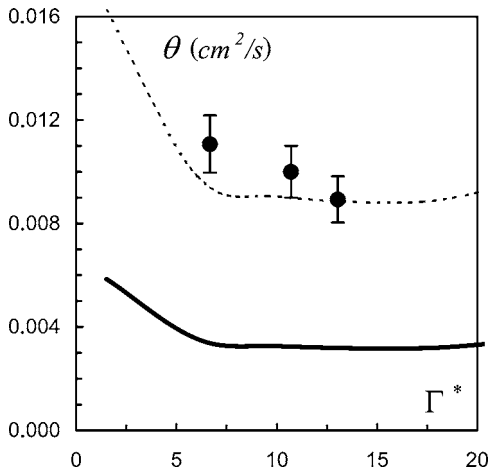

FIG. 8. The functions $\theta(\Gamma^*)$ obtained by the simulations for $\xi=0$ (solid line), for $\xi=4.2$ (dashed line), and in experiments for steady-state (○) and unsteady-state (●) dust structures.

be assured that both this difference and the magnitude of A are absolutely independent on a mechanism of formation of heat sources. In spite of this, the obtained estimation of $\theta \approx 0.014$ cm^2/s is in a good accordance with the results of the determination of thermal diffusivity in the steady state conditions (see Table I).

Notice also that the experimental results are in good agreement with the theoretical estimations from Eq. (2), and with the data of numerical simulation of diffusion coefficients [9–12] (see Fig. 8). The quantitative differences of the measurements from the results of numerical calculations performed for monatomic liquids ($\nu_{fr}=0$, $\xi=0$) may be associated with the processes of dissipation of the energy of macroparticles. If we rely on Eq. (2) and take into account the fact that $D \propto 1/(1+\xi)$, the values of heat transfer coefficients in dissipative systems must exceed their values for the dispersion case by a factor of $(1+\xi)^{5/8}$, i.e., by a factor of ~ 3 for the experimental conditions. The results of numerical calculations for parameter $\xi=4.2$ close to the experimental condition are also shown in Fig. 8. We can see a good agreement of our data with the results of numerical simulations for simple liquids. It should be noted that for the "perfect" (without defects) crystals, the heat transfer coefficients must tend to an infinity because their diffusion constants $D \to 0$ [see Eq. (2)]. The real lattices have usually a few percents of defects, the value of $D \neq 0$, and the heat transfer coefficients have the finite values that, nevertheless, must be higher than those in the liquid state of systems. So, for example, the measurements of thermal diffusivity θ coefficients for the crystalline state of dust structures in rf-discharge, presented in [17] for weakly dissipative system ($\xi \ll 1$), show that the normalized value of thermal diffusivity $\theta^* = \theta/(\omega^* r_d^2) \sim 5-10$ is well above the value of $\theta^* \sim 0.2-0.4$ predicted for the liquid systems with the screened Coulomb potential (see Fig. 1).

Finally we emphasize that here we have observed a heat transfer for the horizontal planes of the dust structures only. (We have not registered any temperature gradients in the vertical direction.) Because of this we do not have any information on the coefficients of heat transfer for the vertical cross section of analyzed structures.

V. EXPERIMENTS IN DUSTY PLASMA IN RF-DISCHARGE UNDER ACTION OF ELECTRON BEAMS

The electron beam is the convenient instrument that allows influencing of dusty plasma structures trapped in a confined electric field of the rf-discharge chamber. This influence results in changing of the parameters of plasma within which under gravitational and electrical force dust macroparticles are levitating. It, in turn, leads to the variations in parameters of dust structures (dust temperatures, concentrations, coupling parameters). (Detailed work devoted to studying the dynamical processes in dusty plasma under the effect of electron beam will be published.)

Here we present the experimental study of heat transfer for macroparticles in rf-discharge plasma under action of electron beam. The scheme of experiment is given in Fig. 9(a). For diagnostics, the particles of a dust cloud were illuminated by a He-Ne laser and filmed (frame frequency $f=50$ s^{-1}). The experiments were performed in air ($P \approx 13$ Pa) with Al_2O_3 particles ($a_d \approx 2$ μm, $\rho_d \approx 2.4$ g cm^{-3}) and latex particles ($a_d \approx 0.5$ μm, $\rho_d \approx 1.5$ g cm^{-3}). Under the experiments, the observed dust clouds were the liquid structures (consisting of ~ 15 dust layers ~ 5 cm in diameter). One of the cloud edges was illuminated by the flat electron beam. A density of electron current j_e in the beam (a power of electron beam) was changed from ~ 0.05 to

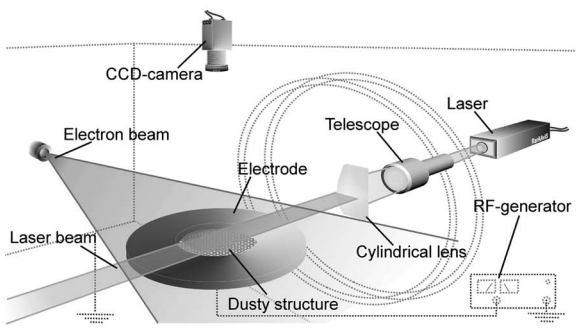

(a)

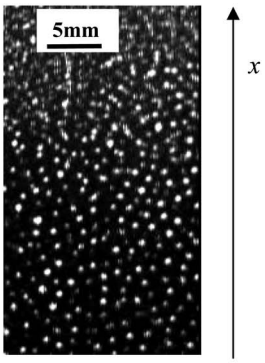

(b)

FIG. 9. The scheme of the experiment (a) and video image of dust structure (b) in plasma with the electron beam.

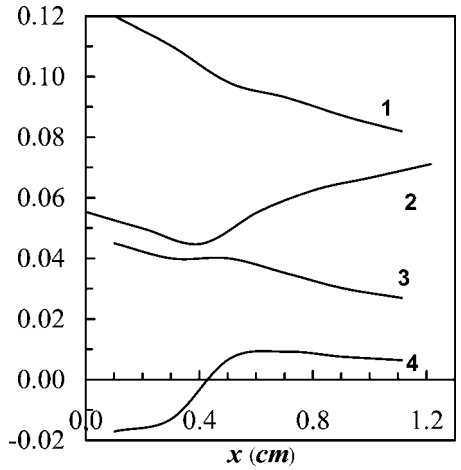

FIG. 10. Dependencies of measured parameters (r_d, T, Γ^*, q) on distance x from the end of the video image (see Fig. 8) toward the electron beam: **1**–r_d, cm; **2**–T, eV; **3**–$\Gamma^*/1000$; and **4**–q/ρ, cm^3/s^3.

~ 0.2 mA/mm^2. A video image of dust structure under the action of electron beam is shown in Fig. 9(b). The dust parameters (temperature, concentration, heat flux, correlation function) changed in the horizontal direction $\boldsymbol{x}$ (perpendicular to the flat of the electron beam) only. We have registered no changes for dust parameters in other directions. The analysis of measured dust velocity distribution functions has also not revealed any convective (or another regular) motion in analyzed structures. Dependencies of measured parameters (r_d, T, Γ^*, q) on distance x from the end of the video image toward the electron beam are shown in Fig. 10 for experiments with latex particles ($j_e \approx 0.1$ mA/mm^2). The values of heat flux density q were determined. Then the values of conductivity χ (from Eq. (3)) and the values of $\theta = 2\chi/(5n_d k_B)$ were obtained. The errors in measured values of θ were less than 30%.

The retrieved values of θ for different experiments are presented in Table II along with the measured mean interparticle distance l_p, dust temperature T, and Γ^*. Normalized thermal diffusion constants $\theta^* = \theta/[(\omega^* r_d^2)(1+\zeta)^{5/8}]$ versus Γ^* are shown in Fig. 11 for numerical calculations and for different experiments. (We can see that the numerical and experimental results agree closely with each other.) The value of ω^* was determined from experimental data (see Table II): $\omega^* = (T\Gamma^*/(\pi M r_d^2)\}^{1/2}$. The friction coefficients (in a free-molecular approach) were $\nu_{fr} \approx 17.5$ s^{-1} for Al_2O_3 particles, and $\nu_{fr} \approx 112$ s^{-1} for latex particles [19].

TABLE II. Thermal diffusion constants θ for different experiments in plasma with electron beam.

T (eV)	Γ^*	r_d (mm)	θ (cm^2/s)
	Al_2O_3 ($j_e \approx 0.1$ mA/mm^2)		
2.0	55	0.71	0.027
2.8	45	0.70	0.024
3.7	29	0.69	0.022
	Latex ($j_e \approx 0.1$ mA/mm^2)		
0.055	45	1.20	0.132
0.050	40	1.10	0.111
0.055	35	0.93	0.080
0.063	30	0.87	0.077
0.067	27	0.82	0.067
	Latex ($j_e \approx 0.05$ mA/mm^2)		
0.027	29	1.10	0.082
0.037	23	0.93	0.080
0.048	19	0.85	0.087
0.050	14	0.81	0.093

VI. ANALYSIS OF EXPERIMENTAL RESULTS AND CONCLUSIONS

Let us take up the possible mechanisms of heat transport in presented experiments. It has been known that heat transport can be effected (i) by the temperature gradients (heat exchange/transfer) via the heat conduction, or the convection and (ii) by the nonuniform distribution of other physical parameters, for example, by the concentration gradients (via the mass transfer/diffusion), or by the external perturbations of an equilibrium field of forces. Here we emphasize that the analysis of measured dust velocity distribution has not revealed any convective (or another regular) motion in analyzed structures for stationary cases as well as for unsteady-state heat transport. Because of these we can suppose that both convections and diffusions are lacking in our experiments. Nevertheless the considered dust structures are open subsystems of the complex dusty plasma system as a whole; and the process of temperature perturbation may by determined by the perturbations of surrounding components of plasma (electrons, ions). It, in turn, can lead to the perturbation of the mean electric fields in the analyzed system as well as to the variations of local electric fields specified by the

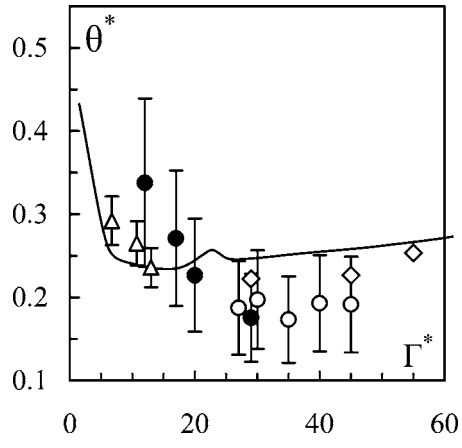

FIG. 11. Normalized thermal diffusion constants θ^* vs Γ^* for numerical calculations (line) and for different experiments in plasma with electron beam: ●–latex, $j_e \approx 0.05$ mA/mm^2; ○–latex, $j_e \approx 0.1$ mA/mm^2; ◇–Al_2O_3 particles, $j_e \approx 0.1$ mA/mm^2; and for Al_2O_3 particles in gas discharge plasma (△) for the stationary case.

interactions between dust particles. However, a presence of any nonbalanced regular component of electric field produces the additional nonbalanced force (not compensated by another forces of system). This force has to lead to a drift motion of dust particles. (Recall that we do not observe this motion.) If we will consider the processes of heat transport (for dusty component) by the heat conduction, the presence of local perturbation of another charged component of plasma determines a potential energy of interparticle interaction (dust charges and type of interparticle potential). It, in turn, effects on the values of measured coefficients of thermal conductivity and thermal diffusivity. Thus it is quite possible that the observed differences between the numerical and experimental results can be associated not only with dissipation processes, but with a discrepancy between the numerical model (assumed the screened Coulomb potential) and the conditions of experiments as well.

In conclusion, we will emphasize that the heat-transfer coefficients for liquid plasma-dust structures were measured. The temperature dependence of these coefficients agrees qualitatively with the results of analysis based on the constancy of relations between the transfer coefficients (D and χ). The quantitative difference of the measurements from the results of numerical calculations performed for monatomic liquids may be caused by the loss of energy of dust particles due to their collisions with neutrals of surrounding gas and also by the discrepancy between the model and experimental potentials.

ACKNOWLEDGMENTS

This work was partially supported by Max Planck Award Cooperation Research, by the Russian Foundation for Basic Research (Grant Nos. 04-02-16362, 06-02-17532, and 06-08-01569), CRDF (Grant No. RU-P2-2593-MO-04), NWO (Grant No. 047.016.020), and by Complex Research Program of the Presidium of Russian Academy of Sciences.

[1] Ya. I. Frenkel', *Kinetic Theory of Liquids* (Clarendon Press, Oxford, 1946).
[2] *Photon Correlation and Light Beating Spectroscopy*, edited by H. Z. Cummins and E. R. Pike (Plenum, New York, 1974).
[3] N. K. Ailawadi, Phys. Rep. **57**, 241 (1980).
[4] N. H. March and M. P. Tosi, *Introduction to Liquid State Physics* (World Scientific, Singapore, 1995).
[5] H. M. Thomas and G. E. Morfill, Nature (London) **379**, 806 (1996).
[6] R. T. Farouki and S. Hamaguchi, Appl. Phys. Lett. **61**, 2973 (1992).
[7] M. O. Robbins, K. Kremer, and G. S. Grest, J. Chem. Phys. **88**, 3286 (1988).
[8] S. Ishimaru, Rev. Mod. Phys. **54**, 1017 (1982).
[9] H. Ohta and S. Hamaguchi, Phys. Plasmas **7**, 4506 (2000).
[10] O. S. Vaulina and S. V. Vladimirov, Phys. Plasmas **9**, 835 (2002).
[11] O. S. Vaulina, S. V. Vladimirov, O. F. Petrov, and V. E. Fortov, Phys. Rev. Lett. **88**, 245002 (2002).
[12] O. S. Vaulina and O. F. Petrov, JETP **99**, 510 (2004).
[13] T. Saigo and S. Hamaguchi, Phys. Plasmas **9**, 1210 (2002).
[14] J. Wallenborn and M. Baus, Phys. Rev. A **18**, 1737 (1978).
[15] Z. Donko and B. Nyiri, Phys. Plasmas **7**, 45 (2000).
[16] V. E. Fortov, O. S. Vaulina, O. F. Petrov *et al.*, Phys. Rev. Lett. **90**, 245005 (2003).
[17] S. Nunomura, D. Samsonov, S. Zhdanov, and G. Morfill, Phys. Rev. Lett. **95**, 025003 (2005).
[18] O. S. Vaulina, O. F. Petrov, V. E. Fortov, A. V. Chernyshev, A. V. Gavrikov, and O. A. Shakhova Phys. Rev. Lett. **93**, 035004 (2004).
[19] U. Konopka, L. Ratke, and H. M. Thomas, Phys. Rev. Lett. **79**, 1269 (1997); U. Konopka, G. E. Morfill, and L. Ratke, *ibid.* **84**, 891 (2000).
[20] V. E. Fortov, O. F. Petrov, A. D. Usachev, and A. V. Zobnin, Phys. Rev. E **70**, 046415 (2004).
[21] V. E. Fortov, A. P. Nefedov, V. I. Molotkov, M. Y. Poustylnik, and V. M. Torchinsky, Phys. Rev. Lett. **87**, 205002 (2001).
[22] G. E. Morfill, V. N. Tsytovich, and H. Thomas, Plasma Phys. Rep. **29**, 1 (2003); S. V. Vladimirov and M. Nambu, Phys. Rev. E **52**, R2172 (1995).
[23] E. M. Lifshitz and L. P. Pitaevskii, *Physical Kinetics* (Pergamon Press, Oxford, 1981).
[24] L. D. Landau and E. M. Lifshitz, *Fluid Mechanics* (Pergamon Press, Oxford, 1987).
[25] V. I. Molotkov, A. P. Nefedov, V. M. Torchinskii *et al.*, JETP **89**, 477 (1999).
[26] V. V. Zhakhovskii, V. I. Molotkov, A. P. Nefedov *et al.*, JETP Lett. **66**, 419 (1997).
[27] O. S. Vaulina, A. A. Samarian, O. F. Petrov *et al.*, Plasma Phys. Rep. **30**, 652 (2004).
[28] O. S. Vaulina, A. A. Samarian, B. James *et al.*, JETP **96**, 1037 (2003).
[29] O. S. Vaulina, S. A. Khrapak, A. P. Nefedov, and O. F. Petrov, Phys. Rev. E **60**, 5959 (1999).
[30] R. A. Quinn and J. Goree, Phys. Rev. E **61**, 3033 (2000).
[31] S. A. Maiorov, S. V. Vladimirov, and N. F. Cramer, Plasma Phys. Rep. **28**, 946 (2002).
[32] S. V. Vladimirov, S. A. Maiorov, and N. F. Cramer, Phys. Rev. E **63**, 045401(R) (2001).
[33] Yu. P. Raizer, *Gas Discharge Physics* (Springer, Berlin, 1991); A. A. Ovchinnikov, S. F. Timashev, and A. A. Belyy, *Kinetics of Diffusion Controlled Chemical Processes* (Nova Science, Commack, NY, 1989).